

# Modelling the redshift-space distortion of galaxy clustering

Steve Hatton<sup>\*</sup> and Shaun Cole<sup>†</sup>

*Department of Physics, University of Durham, Science Laboratories, South Rd, Durham DH1 3LE.*

14 August 2018

## ABSTRACT

We use a set of large, high-resolution cosmological  $N$ -body simulations to examine the redshift-space distortions of galaxy clustering on scales of order  $10 - 200h^{-1}\text{Mpc}$ . Galaxy redshift surveys currently in progress will, on completion, allow us to measure the quadrupole distortion in the 2-point correlation function,  $\xi(\sigma, \pi)$ , or its Fourier transform, the power spectrum,  $P(k, \mu)$ , to a high degree of accuracy. On these scales we typically find a positive quadrupole, as expected for coherent infall onto overdense regions and outflow from underdense regions, but the distortion is substantially weaker than that predicted by pure linear theory. We assess two models that may be regarded as refinements to linear theory, the Zel'dovich approximation and a dispersion model in which the non-linear velocities generated by the formation of virialized groups and clusters are treated as random perturbations to the velocities predicted by linear theory. We find that neither provides an adequate physical description of the clustering pattern. If used to model redshift space distortions on scales for  $10 < \lambda < 200h^{-1}\text{Mpc}$  the estimated value of  $\beta$  ( $\beta = f(\Omega_0)/b$  where  $f(\Omega_0) \approx \Omega_0^{0.6}$  and  $b$  is the galaxy bias parameter) is liable to systematic errors of order ten per cent or more. We discuss how such systematics can be avoided by i) development of a more complete model of redshift distortions and ii) the direct use of galaxy catalogues generated from non-linear  $N$ -body simulations.

**Key words:** cosmology: theory – large-scale structure of Universe – galaxies: clustering – galaxies: distances and redshifts.

## 1 INTRODUCTION

In early galaxy redshift surveys (eg. Jackson 1972; Gregory & Thompson 1978), some of the most striking artefacts observed were the so-called ‘fingers of God’, ridges in the galaxy distribution pointing directly at the observer. What had been observed was the first evidence of the redshift-space distortion of galaxy clustering. If galaxy motions were perfectly described by pure Hubble flow, then a galaxy’s redshift would be an accurate indicator of its distance and the clustering pattern observed in galaxy redshift surveys would be statistically isotropic. The observed anisotropic clustering pattern is generated by galaxy peculiar velocities which perturb galaxy redshifts and hence their inferred distances. On small scales, the non-linear velocities of virialized groups and clusters create the ‘fingers of God’ by stretching out these structures along the line of sight. On large scales the clustering pattern is predicted (as suggested by Sargent & Turner 1977) to be compressed along the line of sight by coherent infall onto galaxy clusters and super-clusters and outflow from

voids and other underdense regions. Thus the anisotropy of galaxy clustering encodes information about the galaxy velocity field and hence the underlying mass density field that gave rise to it. Measurements of redshift-space distortions can therefore be used to place constraints on the density parameter,  $\Omega_0$ , and the bias parameter,  $b$ , which relates the galaxy distribution to the mass distribution.

Interesting constraints on the combination  $\beta \equiv \Omega_0^{0.6}/b$  have been obtained by analysis of optical redshift surveys (Loveday et al. 1996; Ratcliffe et al. 1997a) and IRAS surveys (eg. Hamilton 1993; Fisher et al. 1994; Cole, Fisher & Weinberg 1995 and more recent papers such as Fisher & Nusser 1996; Bromley, Warren & Zurek 1997). However, the statistical errors remain large and no consensus on the value of  $\beta$  has been reached (for a review see Strauss & Willick 1996). The next generation of large surveys, including the 2-degree-Field (2dF, Colless 1996) and Sloan Digital Sky Survey (SDSS, Gunn & Weinberg 1995), will enable redshift-space distortions to be measured with unprecedented accuracy. These surveys should allow  $\beta$  to be measured to an accuracy of a few per cent, and possibly for  $\Omega_0$  and  $b$  to be separately constrained. To achieve this accuracy and avoid systematic errors it is important that the theoretical

<sup>\*</sup> S.J.Hatton@durham.ac.uk

<sup>†</sup> Shaun.Cole@durham.ac.uk

modelling of redshift-space distortions be accurate. This is a non-trivial requirement, as these surveys will provide their most precise measurements of the distortions on scales of 30–100 $h^{-1}$  Mpc, where the predictions of pure linear theory are not expected to hold.

In this paper we use a set of high-resolution  $N$ -body simulations which accurately follow the evolution of clustering over the range of scales which will be probed by the next-generation surveys. Rather than constructing mock galaxy catalogues we instead use the full simulations to quantify the redshift-space distortions as accurately as possible, and through this assess the accuracy of the linear theory model and two proposed extensions to it. In Section 2 we define our notation convention and introduce the quadrupole statistic which we use to assess the level of redshift-space distortion. Section 3 details the parameters of our set of  $N$ -body simulations, and explains the methods we employ to construct biased galaxy samples. The linear theory prediction and the two other models are described in Section 4. In Section 5 we compare the analytic models with measurements of the redshift-space distortions in the  $N$ -body simulations. We discuss results in Section 6.

## 2 ANISOTROPY IN REDSHIFT-SPACE

### 2.1 The power spectrum

Our method of analysis uses the power spectrum,  $P(\mathbf{k})$ , the Fourier transform of the correlation function,

$$P(\mathbf{k}) = \int \xi(\mathbf{r}) e^{i\mathbf{k}\cdot\mathbf{r}} d^3\mathbf{r}, \quad (2.1)$$

where we use the Fourier convention that the wavenumber,  $k$ , is the angular frequency corresponding to wavelength  $\lambda$ , ie.  $k = 2\pi/\lambda$ . The correlation function is given by

$$\xi(\mathbf{r}) = \langle \delta(\mathbf{x} + \mathbf{r})\delta(\mathbf{x}) \rangle, \quad (2.2)$$

where  $\delta(\mathbf{r})$  is the fractional overdensity,

$$\delta(\mathbf{r}) = \frac{\rho(\mathbf{r}) - \bar{\rho}}{\bar{\rho}}. \quad (2.3)$$

The power spectrum has been used by many authors to study the growth of gravitational clustering in simulations, and to quantify the clustering observed in redshift surveys (for recent examples, see da Costa et al. 1994; Tadros & Efstathiou 1995; Lin et al. 1996).

When galaxy distances are measured in redshift space, their peculiar velocities (ie. relative to the pure Hubble flow) distort the pattern of galaxy clustering by displacing galaxy positions along the line of sight. Thus a galaxy whose true position is  $\mathbf{r}$  appears in redshift-space at the position

$$\mathbf{s} = \mathbf{r} + U(\mathbf{r})\hat{\mathbf{r}}, \quad (2.4)$$

where the line-of-sight peculiar velocity  $U(\mathbf{r}) = \mathbf{v}(\mathbf{r})\cdot\hat{\mathbf{r}}$ . Here we have adopted units in which the Hubble constant has unit value, we measure distance in units of  $h^{-1}$  Mpc, where  $h \equiv H_0/(100\text{km s}^{-1}\text{Mpc}^{-1})$ , and velocities in units of  $100\text{km s}^{-1}$ .

In redshift space this displacement in a preferred direction causes the observed power spectrum to be anisotropic, with different values for wave-vectors along the line of sight to those perpendicular to it. Thus, the redshift-space power spectrum can be thought of as a function of  $k$  ( $= |\mathbf{k}|$ ) and  $\mu$ ,

the cosine of the angle between wave-vector  $\mathbf{k}$  and the line of sight,

$$P(\mathbf{k}) = P(k, \mu). \quad (2.5)$$

In what follows we adopt the convention that, by  $P(\mathbf{k})$  or  $P(k, \mu)$  we refer to the redshift-space power spectrum, since this quantity depends on both the magnitude and direction of  $\mathbf{k}$ , whereas  $P(k)$  represents the real space power spectrum, depending only on the scalar  $k$ .

### 2.2 The quadrupole ratio

The redshift-space distortions can be conveniently quantified by a simple statistic. The anisotropy in  $P(\mathbf{k})$  is symmetric in  $\mu$ , ie.  $P(k, \mu) = P(k, -\mu)$ , so the distortion depends only on even powers of  $\mu$ . To measure the extent of deformation from isotropy, we decompose the power spectrum into multipole moments using the Legendre polynomials,  $L_l(\mu)$ . Thus,

$$P(k, \mu) = \sum_{l=0}^{\infty} P_l(k) L_l(\mu), \quad (2.6)$$

where the sum is over even values of  $l$ . From the orthogonality relation for Legendre Polynomials, the multipole moments  $P_l(k)$  can be found by evaluating

$$P_l(k) = \frac{2l+1}{2} \int_{-1}^{+1} P(k, \mu) L_l(\mu) d\mu. \quad (2.7)$$

We find that estimates of  $P_l(k)$  rapidly become noisy for multipoles with  $l > 2$ , so we choose to use as the key statistic for our analysis the quadrupole to monopole ratio,  $P_2(k)/P_0(k)$ .

We have chosen to carry out all our analysis in  $k$ -space using power spectrum multipoles  $P_l(k)$ . However, our results can readily be translated into predictions of the multipole moments of the correlation function,  $\xi_l(r)$  using the identities derived in appendix B of Cole, Fisher & Weinberg (1994).

## 3 SIMULATIONS

In order to study the effects of non-linear gravitational evolution on redshift space clustering we examine a selection of  $N$ -body simulations with different values of the density parameter  $\Omega_0$  and the galaxy bias. The simulations we use are taken from a set of large volume simulations which have been produced in order to make mock redshift catalogues of the Sloan Digital Sky Survey (Gunn & Weinberg 1995) and the Anglo-Australian 2-Degree Field Survey (Colless 1996), as will be described in Cole, Weinberg, Hatton & Frenk (in preparation). The full set of simulations consists of two series. The first is normalized to the amplitude of CMB fluctuations in the COBE-DMR data set (Smoot et al. 1992) and the second normalized to match present day observations of galaxy clusters and large scale structure. Both series cover a range in  $\Omega_0$  and include both open models (with  $\Lambda_0 = 0$ ), and flat models ( $\Omega_0 + \Lambda_0 = 1$ , where  $\Lambda_0$  is the cosmological constant in units of  $3H_0^2$ ).

The main cause of redshift-space distortion on small scales is the random velocities of galaxies in groups and clusters. Since our aim is to study deviations from linear theory

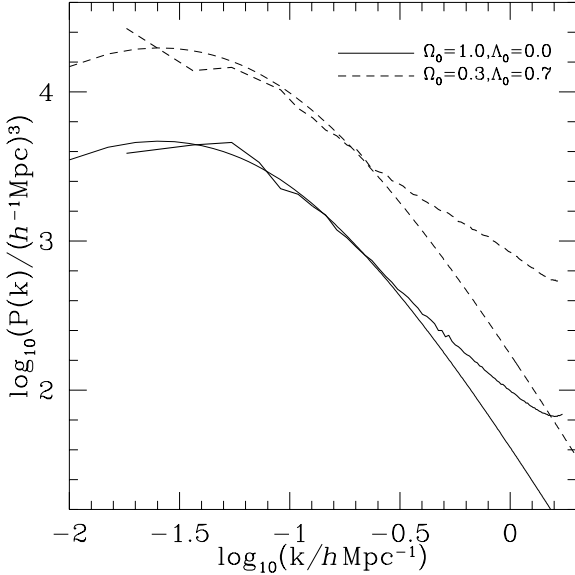


**Figure 1.** Power spectra of the real-space mass distributions of the  $N$ -body simulations described in Section 3. In each case the thin line is the linear theory,  $\Gamma = 0.25$  CDM spectrum (3.1) which was used to set up the initial conditions of the simulations, the thicker line is the evolved, non-linear power spectrum of the simulation measured at  $z = 0$ .

on scales of  $10\text{--}200h^{-1}$  Mpc this important non-linear effect must be included at a realistic level. Therefore we have selected simulations from the series that are normalized to produce approximately the observed abundance of rich galaxy clusters. This set of simulations have the rms mass fluctuation in spheres of radius  $8h^{-1}$  Mpc set to  $\sigma_8 = 0.55\Omega_0^{-0.6}$  (White, Efstathiou & Frenk 1993). The shape of the initial power spectrum is the same in each simulation and is given by the Bardeen et al. (1986) formula for the cold dark matter spectrum,

$$P(k) \propto \frac{k \times [\ln(1 + 2.34q)/2.34q]^2}{[1 + 3.89q + (16.1q)^2 + (5.46q)^3 + (6.71q)^4]^{1/2}}. \quad (3.1)$$

Here  $q = k/\Gamma$  and we set  $\Gamma = 0.25$ , as suggested by observations of large scale structure (eg. Feldman, Kaiser & Peacock 1994; Maddox, Efstathiou & Sutherland 1996). To illustrate our results we focus mainly on two models, the  $\Omega_0 = 1$  model and a low density  $\Omega_0 = 0.3$ ,  $\Lambda_0 = 0.7$  model.

The initial particle positions and velocities were set by using the Zel’dovich (1970) approximation to perturb particles from an almost uniform “glass” distribution. This “glass” distribution was produced using the technique described by White (1994), and Baugh, Gaztañaga & Efstathiou (1995). The simulations were evolved using the AP<sup>3</sup>M code of Couchman (1991) using  $192^3$  particles in a periodic cube of side  $L_{\text{box}} = 345.6h^{-1}$  Mpc (comoving distance). The softening parameter of AP<sup>3</sup>M’s triangular-shaped cloud force law was set to  $\eta = 270h^{-1}$  kpc, 15 per cent of the grid spacing. This choice corresponds approximately to a gravitational softening length  $\epsilon = \eta/3 = 90h^{-1}$  kpc for a Plummer force law. Further details and some analysis of these simulations can be found in Eke, Cole & Frenk (1996) and in Cole et al. (in preparation).

### 3.1 Biased Galaxy Catalogues

Results from recent galaxy surveys suggest that galaxies do not perfectly trace the mass distribution but rather pick out the highly non-linear regions. For instance, Peacock & Dodds (1994) show there are in fact different bias factors for differently selected galaxy samples, eg. IRAS galaxies and radio galaxies. Many of these recent investigations favour a value of  $\beta \approx 0.5$ , so for a flat universe with zero cosmological constant a significant amount of biasing is needed to match observations. To this end we employ three different methods of biasing our  $\Omega_0 = 1.0$  simulation, in order to find out how robust our parameter estimation techniques are to the precise bias prescription.

In each method we build up a ‘probability field’ on a grid, based on the density field smoothed on a particular scale. We then randomly sample the particles using the values of the probability field at their nearest grid points as their Poisson mean probability of being selected as galaxies.

The first two methods we employ are Lagrangian, in the sense that the selection probability is based on the *initial* density field. The third is an Eulerian one, where the galaxy distribution is ‘painted on’ depending on the final, evolved density field. In each case the bias is chosen to obtain a  $\sigma_8^{\text{gal}}$ , the variance in galaxy counts in spheres of radius  $8h^{-1}$  Mpc, consistent with the results of Maddox, Efstathiou & Sutherland (1996), who find  $\sigma_8^{\text{gal}} = 0.96$  for the APM Galaxy Survey. Thus, the bias factor, defined as  $\sigma_8^{\text{gal}}/\sigma_8$ , has value  $b = 1.81$ . All our methods are local schemes based on the value of the overdensity at a given point. The methods are expected to produce a constant bias on large scales.

**Method 1** High Peaks Biasing. For this method we smooth the initial density field by applying a sharp cut-off in the power at a scale  $r_s$ , set to be, approximately, the shortest resolvable wavelength in the box,  $r_s \approx 4h^{-1}$  Mpc. We then divide by the resulting mass variance,  $\sigma_s$ , to obtain a new variable,  $\nu(\mathbf{r}) = \delta(\mathbf{r})/\sigma_s$ . We use the results of Bardeen et al. (1986) to calculate the mean number of peaks above a certain threshold,  $\nu_r$ , for a random field, Gaussian-smoothed on a scale  $r_{\text{gal}} = 0.54h^{-1}$  Mpc, ie. the number of galaxy-scale peaks expected as a function of  $\nu$  (cf. White et al. 1987). The value of the threshold is adjusted until the required level of bias is obtained, from  $\sigma_8^{\text{gal}} = b\sigma_8$ . We find that  $\nu_r = 0.99$  gives the correct normalization.

**Method 2** For this method we obtain  $\nu(\mathbf{r})$  by smoothing the initial density with a Gaussian of scale  $r_s = 5h^{-1}$  Mpc. Our biasing probability field is then a continuous function of  $\nu$  and two adjustable parameters,  $\alpha$  and  $\beta$ , given by

$$P(\nu) = A \exp(\alpha\nu + \beta\nu|\nu|) \quad (3.2)$$

where the normalization constant,  $A$ , is determined by the constraint

$$\int P(\nu) \frac{\exp(-\nu^2/2)}{\sqrt{2\pi}} d\nu = 1. \quad (3.3)$$

In the limit of small ( $\delta \ll 1$ ) large-scale perturbations in the initial density field, it can be shown that the bias on large scales is given by

$$b = 1 + \frac{\alpha}{\sigma_s} + \frac{2\beta}{\sigma_s} \int P(\nu) |\nu| \frac{\exp(-\nu^2/2)}{\sqrt{2\pi}} d\nu. \quad (3.4)$$

To fix  $\alpha$  and  $\beta$  we demand that the rms galaxy density fluctuation

tuations in two different sized cubic cells (5 and  $20h^{-1}$  Mpc) match those predicted by assuming a power spectrum shape from the result for the APM survey found by Baugh & Gaztañaga (1996).

**Method 3** In this model the final density field is smoothed on a scale  $r_s = 5h^{-1}$  Mpc. The selection probability field has a value 0 or 1 according to whether the overdensity is below or above a threshold,  $\tau$ . We find that  $\tau = 1.53$  provides the required bias. The particle distribution resulting from this scheme is expected to contain large voids since the sharp cut-off at the threshold is extremely effective at evacuating underdense regions (Weinberg & Cole 1992).

It is hoped that the three methods described here span a broad range of plausible biasing prescriptions that might occur in the real universe, and that, if we can develop techniques that are unaffected by which of these schemes is chosen, these techniques will be insensitive to the way in which bias comes about. Further details about biasing schemes will follow in Cole et al. (in preparation).

The density of the biased catalogues is chosen to be one galaxy per  $25(h^{-1} \text{Mpc})^3$ , roughly four times  $\phi_*$ , the observed number density of  $L_*$  galaxies (eg. Peebles 1993, §5; Ratcliffe et al. 1997b). This high sampling density has been adopted as we are interested in investigating systematic effects on the redshift-space distortions, and so we want to minimize the statistical uncertainties produced by sparse sampling.

### 3.2 Zel'dovich approximation simulations

We attempt to model the redshift-space distortions in our  $N$ -body simulations using a Monte Carlo implementation of the Zel'dovich approximation. Our Monte Carlo realizations have the same  $192^3$  particle grid and initial density field parameters as the corresponding  $N$ -body simulations. Exactly the same method is used to perturb the particles as that employed to get the initial displacements in the  $N$ -body simulation, only with much larger perturbation amplitude corresponding to  $z = 0$  rather than the starting redshift of the simulation. For the  $N$ -body simulations we populate all the modes in the  $192^3$   $k$ -space grid including those in the corners of the cube. However for these realizations of the ZA, we make our treatment consistent with the analytic calculation that we outline in Section 4.3, by smoothing the density field in the same way, ie. by truncating the power spectrum isotropically at  $k_{\text{Nq}} = 1.743h \text{Mpc}^{-1}$ .

These realizations of the ZA can be biased using exactly the same prescriptions that we use for the  $N$ -body simulations. The catalogues thus created are then subjected to the same multipole analysis as our  $N$ -body simulations.

### 3.3 Estimation of multipole moments

We ensure that the distant observer approximation is satisfied by assigning redshift-space positions to galaxies based on their distance along the  $x$ -axis of the simulation. Effectively the simulation box is placed at infinity and the line of sight aligned with the  $x$ -axis. To minimise the noise in our estimates we repeat the analysis with the simulation ro-

tated to align the line of sight with the  $y$ - and then  $z$ -axes and average the results.

The galaxies in the simulation are assigned to a  $192^3$  grid using the cloud-in-cell (CIC) weighting scheme (Efstathiou et al. 1985). The density field thus produced then has the average galaxy density subtracted from it and is divided by this average density. The resultant grid is thus the fractional overdensity field,  $\delta(\mathbf{r})$ , and the grid is fast Fourier transformed to get  $\delta(\mathbf{k})$ . The effect of the CIC assignment is to doubly convolve the density field with the shape of a grid cell. Thus to deconvolve we divide by the square of Fourier transform of the CIC window function. The power spectrum estimator is then  $\delta(\mathbf{k})\delta(\mathbf{k})^*$ .

For the biased galaxy simulations a constant equal to the inverse of the number density of galaxies in the catalogue is subtracted at this point to account for the shot noise introduced by the Poisson sampling of the galaxies. This is not necessary in the unbiased cases as here we use all the particles rather than a Poisson sample.

We now divide  $k$ -space in spherical shells of width  $\Delta k = 2\pi/L_{\text{box}}$ . For each shell we estimate the multipole moments of the power spectrum by approximating the integral of  $\mu$  in (2.7) by a discrete sum over modes. This method works perfectly well at high- $k$ , but for the first few shells where the sampling of  $k$ -space results in poor sampling in  $\mu$  it leads to a small systematic error in  $P_2(k)/P_0(k)$ . An alternative method of estimating  $P_2(k)$  and  $P_0(k)$ , which can readily be employed for low- $k$ , is to make a least squares fit to the  $\mu$  dependence of  $P(k, \mu)$  using a basis of the Legendre polynomials  $L_0, L_2$  and  $L_4$ . This second method produces a less noisy estimator but still suffers from a small systematic error due to the poor sampling in  $\mu$ . We therefore apply a small (5% for the lowest wavenumber), empirically derived correction to our first five bins in  $k$  to compensate for this.

The lowest  $k$ -mode probed using this method is  $k = (2\pi/L_{\text{box}})$ , ie. when one wavelength fills the whole box. The highest is the Nyquist frequency,  $k_{\text{Nq}} = (2\pi/L_{\text{box}})(N/2)$ , where  $N$  is the number of cells along one side of the simulation box. We do not expect our treatment to work all the way up to the Nyquist frequency, since the deconvolution correction can never recover all the information lost by assigning particles to a discrete grid. This effect can be seen in Fig. 1 where the power spectrum turns up for the very highest  $k$ -values. For this reason we limit our analysis rather conservatively to modes with  $k < \frac{1}{2}k_{\text{Nq}}$ .

## 4 ANALYTIC MODELS

If it is assumed that the velocity field,  $\mathbf{v}(\mathbf{r})$ , is generated via gravitational instability, then it can be related to the underlying mass density field. Here we consider three analytic models for the relationship of the velocity field to the density field, which lead to quantitative descriptions of the redshift-space distortion of galaxy clustering. The first is based purely on linear theory. In the second, the effect of non-linear velocities in galaxy clusters is modelled by adding a random velocity dispersion to the velocity predicted by linear theory. The magnitude of this dispersion,  $\sigma_v$ , is not predicted by the model, but is expected to bear some relation to the typical thermal velocity of galaxies within groups and clusters. The third model is the Zel'dovich approximation (ZA)

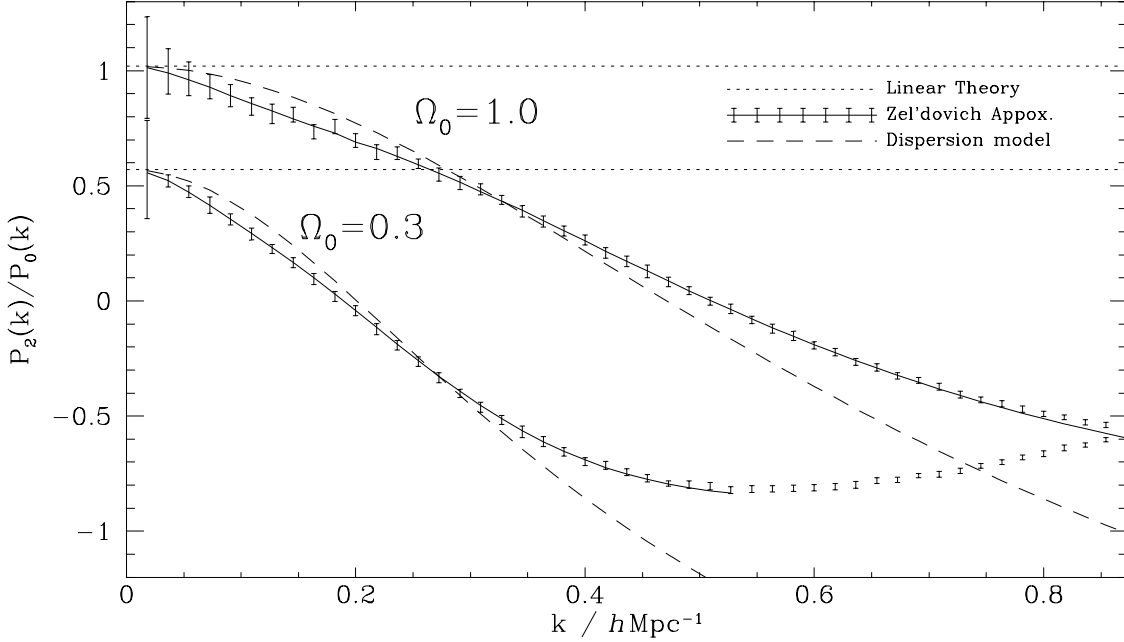


**Figure 2.** Model predictions for the redshift space power spectrum quadrupole to monopole ratio  $P_2(k)/P_0(k)$ . The two sets of curves are for two unbiased ( $b = 1$ ) CDM models with  $\Gamma = 0.25$  power spectra. The upper curves are for  $\Omega_0 = 1.0$ ,  $\sigma_8 = 0.55$ , while the lower model is  $\Omega_0 = 0.3$ ,  $\Lambda_0 = 0.7$  and  $\sigma_8 = 1.13$ . In both cases the curves show the constant ratio predicted by linear theory (dotted), the analytic Zel'dovich Approximation result (solid), and examples of the dispersion model (dashed) with  $\sigma_v = 300 \text{ km s}^{-1}$  for  $\Omega_0 = 1.0$  and  $\sigma_v = 500 \text{ km s}^{-1}$  for  $\Omega_0 = 0.3$ . The error bars show the result of averaging forty random Monte Carlo realizations of the Zel'dovich Approximation. These error bars indicate the standard deviation of the sample, and thus are typical of the error expected in a single realization.

(Zel'dovich 1970). This model provides a complete description of the evolved density and velocity fields, which is expected to be accurate in the quasi-linear regime where the overdensity is of order unity. Thus this model has the potential to give an accurate physical description of redshift-space clustering. These three models are described in detail below and compared in Fig. 2. In each case we assume that the distant observer approximation is well satisfied and that we are dealing with volume limited galaxy samples. The effects of relaxing these assumptions are discussed in Kaiser (1987).

#### 4.1 Linear Theory

In the regime of linear theory Kaiser (1987) showed that the redshift-space power spectrum is related to the real space power spectrum in a very simple way

$$P(k, \mu) = P(k)(1 + \beta\mu^2)^2, \quad \beta \equiv f(\Omega_0)/b \approx \Omega_0^{0.6}/b. \quad (4.1)$$

The function  $f(\Omega_0) \approx \Omega_0^{0.6}$  is the logarithmic derivative of the fluctuation growth rate (see Peebles 1993, §14; Bouchet et al. 1995). The bias factor,  $b$ , is an assumed constant relating fluctuations in the galaxy density to those in the mass.

Applying (2.7) for the  $l = 0$  and  $l = 2$  modes results in

$$\frac{P_2}{P_0} = \frac{4\beta/3 + 4\beta^2/7}{1 + 2\beta/3 + \beta^2/5}. \quad (4.2)$$

Thus linear theory predicts a constant quadrupole-to-monopole ratio,  $P_2/P_0$ , independent of scale. This model is shown by the dotted lines in Fig. 2.

Here we highlight some of the steps in this derivation so that we can compare its assumptions with those of two other proposed models. In linear theory the velocity and galaxy density fields are related by the first order continuity equation,

$$\nabla \cdot \mathbf{v}(\mathbf{r}) = -\beta\delta(\mathbf{r}). \quad (4.3)$$

Considering the density field as a sum over Fourier components,

$$\delta(\mathbf{r}) = \sum \delta(\mathbf{k})e^{-i\mathbf{k} \cdot \mathbf{r}}, \quad (4.4)$$

the resulting linear theory prediction for the velocity field is

$$\mathbf{v}(\mathbf{r}) = -\beta \sum \frac{i\mathbf{k}}{k^2} \delta(\mathbf{k})e^{-i\mathbf{k} \cdot \mathbf{r}}, \quad (4.5)$$

where we have assumed a linear bias between the galaxy and mass density perturbations,  $\delta(\mathbf{r}) = b\delta_{\text{mass}}(\mathbf{r})$ . This leads to the following expression for the line-of-sight velocity gradient,

$$\frac{dU}{dr} = -\beta\mu^2\delta(\mathbf{r}). \quad (4.6)$$

The results (4.1) and (4.2) are valid only so long as each of the four following constraints is satisfied, so that the corresponding form of non-linearity can be ignored (Cole et al. 1994, section 2.2);

1. **dispersion:** The velocity dispersion in virialized systems is sufficiently small that it can be ignored, i.e.  $k\sigma_v \ll 1$

2. **dynamical:** The linear relationship between velocity and overdensity (4.5) is accurate.

3. **gradient:** Second order terms in the gradient of the line-of-sight velocity field can be ignored, i.e.  $dU/dr \ll 1$

4. **contrast:** Second order terms in the galaxy overdensity can be ignored,  $\delta(\mathbf{r}) \ll 1$

All these constraints will be satisfied on the very largest scales, but, depending on the present-day amplitude of galaxy clustering and on the values of  $\Omega_0$  and  $b$ , we expect some or even all of them to be violated on scales of less than  $100h^{-1}$  Mpc.

## 4.2 Linear Theory Plus Dispersion

The velocity dispersion of galaxies in galaxy clusters is typically  $800\text{km s}^{-1}$  (eg. White et al. 1993). Thus, from the the constraint that  $k\sigma_v \ll 1$ , we would expect the linear theory result (4.1) to apply only on scales where  $k \ll 0.125h\text{Mpc}^{-1}$ . Since we are interested in clustering on scales from  $10 - 200h^{-1}\text{Mpc}$  ( $0.03 \lesssim k \lesssim 0.6h\text{Mpc}^{-1}$ ), an accurate model will have to take into account these non-linear velocities.

On small scales the redshift space correlation function has been found to be well modelled as a convolution of the real-space isotropic correlation function with an exponential probability distribution function for line-of-sight velocities (Bean et al. 1983; Davis & Peebles 1983; Fisher et al. 1994).

Park et al. (1994) point out that, since the convolution in  $r$ -space is equivalent to a multiplication in  $k$ -space, the power spectrum is multiplied by the square of the Fourier transform of the velocity distribution function. Peacock & Dodds (1994) show that the effects of linear clustering and this model of small-scale velocity dispersion can be combined to give a redshift space power spectrum

$$P(k, \mu) = P(k)(1 + \beta\mu^2)^2 \left(1 + \frac{(k\mu\sigma_v)^2}{2}\right)^{-2}. \quad (4.7)$$

For this expression it is considerably harder to perform the integration over  $\mu$  required in (2.7) than for the linear theory case, but an analytic expression for  $P_2(k)/P_0(k)$  can easily be obtained with the aid of mathematics packages such as Maple. The rather lengthy formulae are given in Cole et al. (1995) section 2.1.

This model extends linear theory by relaxing the dispersion constraint listed in the previous section, but still implicitly assumes the other three. The model of the small-scale velocity dispersion is also simplistic in that it takes no account of the fact that the velocity dispersion is correlated with the density field, ie. the dispersion is higher in high density regions such as galaxy clusters. This means that the value of  $\sigma_v$  used in this model is only an *effective* velocity dispersion which depends on how galaxies populate the clusters, and thus on the bias parameter,  $b$ . Examples of this model are shown by the short dashed curves in Fig. 2.

## 4.3 The Zel'dovich Approximation

The linear theory approach to modelling the growth of density perturbations is only valid if  $\delta(\mathbf{r}) \ll 1$ . The refinement to linear theory proposed by Zel'dovich (1970) was to formulate a Lagrangian approach. Here each particle is displaced

from its original position along a straight line defined by the direction of the initial velocity field. In comoving coordinates  $\mathbf{r}$ , the final position, is related to  $\mathbf{q}$ , the initial position, by

$$\mathbf{r} = \mathbf{q} + \mathbf{d}(\mathbf{q}, t), \quad \mathbf{d}(\mathbf{q}, t) = \frac{\mathbf{v}(\mathbf{q})}{f(\Omega_0)}. \quad (4.8)$$

The Zel'dovich Approximation (ZA) is expected to break down at the stage when shell-crossing occurs ( $\delta(\mathbf{r}) \sim 1$ ). This is because, under this model, the particles pass right through caustics as they continue to move in the direction of their original velocity. In contrast, in  $N$ -body simulations non-linear effects cause the particles to behave as if they were 'sticky', and galaxies congregate in high density shells or walls. If the power spectrum is not truncated or filtered at high spatial frequencies, shell-crossing occurs on small scales, with the result that small-scale and some large-scale power is erased, and the degree of anisotropy is lower than expected. We choose to smooth the initial density field for the Zel'dovich realizations on small scales by applying a sharp cut-off to the power spectrum at  $k_T = 1.743h\text{Mpc}^{-1}$ , which corresponds to the Nyquist frequency of the grid used in the  $N$ -body simulations.

Fisher & Nusser (1996, henceforth FN96) and Taylor & Hamilton (1996) obtained an analytic result for the redshift-space distortion produced with the ZA. Following their work we have developed an integration technique using an Euler method (Press et al. 1992) to deal with diverging oscillations of the integrand. Over the range of  $k$  we are interested in, the method is quite stable, and avoids the complexity described in the appendix of Taylor & Hamilton (1996). However, our technique breaks down at a scale  $k \gtrsim 0.6/\sigma_8$ . At this point oscillations in the radial integrand become too rapid and of too great an amplitude for the method to cope.

This analytic calculation of the quadrupole ratio  $P_2(k)/P_0(k)$  is compared with the results of averaging many Monte Carlo realizations of the ZA in Fig. 2. The close agreement of the two methods is very reassuring. It not only demonstrates the accuracy of our numerical integration technique, but also our implementation of realizations of the ZA and the entire procedure of estimating  $P_2(k)/P_0(k)$  from particle distributions.

In Fig. 2 the  $P_2/P_0$  ratio of the  $\Omega_0 = 0.3$  model reaches a minimum at  $k \approx 0.5h\text{Mpc}^{-1}$  and then slowly increases. The ratio behaves in a similar manner for  $\Omega_0 = 1.0$ , but with a minimum at  $k \approx 0.95h\text{Mpc}^{-1}$ , which lies off the right-hand side of Fig. 2. We attribute this behaviour to the breakdown of the ZA at scales on which substantial shell crossing has occurred. This occurs on larger scales in the  $\Omega_0 = 0.3$  model as it has the larger amplitude of density fluctuations with  $\sigma_8 = 1.13$  compared with  $\sigma_8 = 0.55$  in the  $\Omega_0 = 1.0$  model. In reality one expects the ratio  $P_2(k)/P_0(k)$  to become increasingly negative on small scales due to the fingers-of-god produced by the random velocities of galaxies in virialized groups and clusters.

In our implementation of the ZA we have applied very little smoothing of the initial density field. We have simply truncated the input power spectrum at the Nyquist frequency of our particle grid used in the Monte Carlo realizations described in Section 3.2 to facilitate inter-comparison. However, Melott, Pellman & Shandarin (1994) have shown that, at least for some statistics, the correspondence between

the ZA and  $N$ -body simulations can be improved by more severe smoothing of the initial density field. They define a non-linear wavenumber  $k_{\text{nl}}$  by

$$4\pi \int_0^{k_{\text{nl}}} P(k)k^2 dk = 1 \quad (4.9)$$

and then smooth the initial density field with a Gaussian window,  $\exp(-k^2/2k_s^2)$ , with  $k_s = pk_{\text{nl}}$ . They find that the best choice of the parameter  $p$  depends only weakly on the shape of the power spectrum and is  $p \simeq 1.25$ . When comparing to the  $N$ -body simulations in Section 5 we investigate whether this procedure improves the redshift space predictions of the ZA.

The ZA has several advantages over pure linear theory. Firstly, equation (4.5) is modified such that the velocity  $\mathbf{v}(\mathbf{r})$  is given in terms of the density field at the initial position  $\mathbf{q}$ , ie.  $\mathbf{r}$  is replaced by  $\mathbf{q}$  in (4.4), and on the right-hand-side of (4.5). This dynamical relation remains quite accurate until shell crossing occurs, whereas the linear theory relation is only accurate for  $\delta(\mathbf{r}) \ll 1$ . In contrast to the linear theory derivation, no further assumptions regarding either the amplitude of the velocity gradient nor the density fluctuations are made in deriving the resulting power spectrum. Thus in this respect it is able to deal with both gradient and contrast non-linearity. For modelling redshift-space distortions the main shortcoming of the ZA is that it does not model the random velocities produced in non-linear relaxed structures – instead it produces its own velocity dispersion on small scales due to the shell crossing. Thus in this respect it does not deal with the dispersion non-linearity. Also in the form described above it does not explicitly deal with the effects of biasing. Fisher & Nusser (1996) claim that to a good approximation bias can be modelled by simply replacing  $f(\Omega_0)$  with  $\beta = f(\Omega_0)/b$  – we investigate this in Section 5.

#### 4.4 Fitting the models

Our objective is to illustrate the systematic differences between the  $N$ -body results and the models rather than to propose a methodology to estimate model parameters from real estimates of the redshift-space distortion. In order to analyze the data from our simulations on quasi-linear scales, we will perform  $\chi^2$  fits for the dispersion and ZA models to the  $N$ -body points and restrict the range of  $k$  to the regime over which each model can reasonably match the data.

The dispersion model provides a functional form for the shape of the quadrupole estimator, but says nothing about the clustering itself. Thus, in fitting to the data, no assumptions need be made about the shape or amplitude of the underlying power spectrum, we simply do a  $\chi^2$  minimization using  $\beta$  and  $\sigma_v$  as fitting parameters.

In contrast, the ZA is much more physically motivated in that it attempts to model both the clustering and the associated velocity field from first principles. We first attempt to utilize a simple fitting formula for the shape of  $P_2(k)/P_0(k)$  presented in FN96. This formula depends on  $\beta$  and the zero-crossing of the quadrupole,  $k_{\text{nl}}$ . We find that using this approximation introduces a significant offset between the best-fit and true values of  $\beta$ . We therefore opt to evaluate the full expression derived by FN96 for the expected quadrupole to monopole ratio at each stage in making the

minimum- $\chi^2$  fit. This expression gives the distortion as a function of  $\beta$  and the power spectrum shape and normalization ( $\Gamma$  and  $\sigma_8$ ). Here we simply adopt the values of  $\Gamma$  and  $\sigma_8$  used in the simulations and use  $\beta$  as the single free parameter in the model. For real observations it is hoped that one could simultaneously fit for these parameters using estimates of the redshift-space power spectrum,  $P_0(k)$ .

## 5 RESULTS

### 5.1 Unbiased Models

In Fig. 3 we compare the model predictions for the quadrupole ratio,  $P_2(k)/P_0(k)$ , with the results of two unbiased  $N$ -body simulations. The points with error bars show the  $N$ -body results. The model that produces the lower quadrupole ratios has  $\Omega_0 = 0.3$ ,  $\Lambda_0 = 0.7$  and  $\sigma_8 = 1.13$ , and that with the stronger quadrupole signal has  $\Omega_0 = 1$  and  $\sigma_8 = 0.55$ . The error bars placed on the  $N$ -body results are indicative of the statistical error we expect on an estimate of the quadrupole ratio, from a single realization, and are obtained by taking the standard deviation of forty Monte Carlo realizations of the ZA. It is clear that, apart from the first few points with  $k \lesssim 0.07h \text{ Mpc}^{-1}$ , the deviation from the constant ratio predicted by linear theory is large.

The solid lines in Fig. 3 are each for one ZA realization starting from the same initial density field as the corresponding  $N$ -body simulation. This model reproduces the  $N$ -body results extremely accurately at low- $k$ . For the  $\Omega_0 = 0.3$  case the ZA and  $N$ -body results match well up to  $k \approx 0.25h \text{ Mpc}^{-1}$  which is beyond the scale at which  $P_2(k)/P_0(k)$  becomes negative. This result is in complete agreement with the findings of FN96. The only  $N$ -body results they studied were for a similarly normalized  $\Omega_0 = 0.3, \Lambda_0 = 0.7$  model. In the case of  $\Omega_0 = 1$  we find much less impressive agreement between the ZA and  $N$ -body simulations. The results begin to diverge at  $k \gtrsim 0.15h \text{ Mpc}^{-1}$  and differ very significantly at  $k = 0.425h \text{ Mpc}^{-1}$ , where  $P_2(k)/P_0(k) = 0$  for the  $N$ -body simulation.

In Fig. 4 we show another comparison between these  $N$ -body and ZA realizations. Here we show the ratio of estimates of their final power spectra to the initial power spectra evolved to  $z = 0$  assuming linear theory. We see that in the  $N$ -body simulations the non-linear growth of structure leads to an increase in power on small scales. This is strongest for  $\Omega_0 = 0.3$  which has the highest  $\sigma_8$  and is therefore the most non-linear. In contrast the behaviour of the ZA simulations is the exact opposite – shell crossing erases power on small scales. In this respect the agreement between ZA and  $N$ -body is particularly poor for the  $\Omega_0 = 0.3$  model. Even at mildly non-linear scales this discrepancy is quite severe, which suggests to us that the success of the ZA at modelling the ratio  $P_2(k)/P_0(k)$  should be treated with skepticism.

The possibility of improving the correspondence with the  $N$ -body results by smoothing the initial density field before applying the ZA, as in the truncated ZA of Melott et al. (1994), is investigated in Fig. 5. The introduction of additional smoothing worsens the agreement between the  $N$ -body results and those of the ZA. In particular for the degree of smoothing advocated by Melott et al., corresponding to  $p \approx 1.25$ , the agreement between  $N$ -body and ZA is very

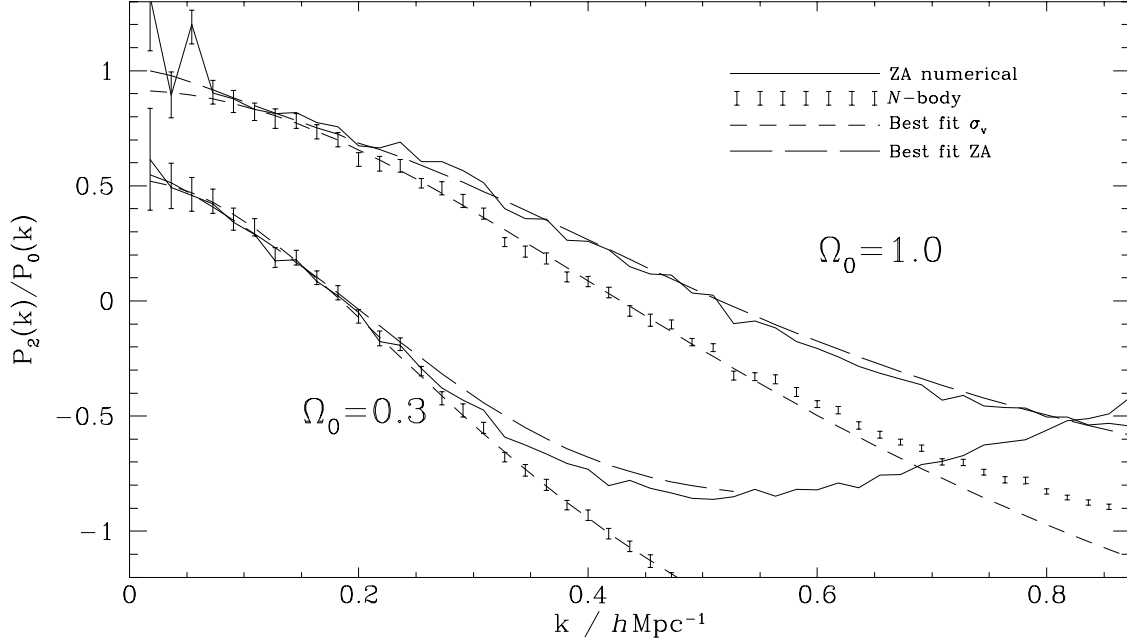


**Figure 3.** The quadrupole ratio  $P_2(k)/P_0(k)$  for two unbiased  $N$ -body simulations compared with the corresponding Zel'dovich approximation simulations and two model fits. The upper curves are for  $\Omega_0 = 1$  and  $\sigma_8 = 0.55$  and the lower curves for  $\Omega_0 = 0.3$ ,  $\Lambda_0 = 0.7$  and  $\sigma_8 = 1.13$ . The error bars on the  $N$ -body results are indicative of the statistical error in our estimates and are estimated from the standard deviation between forty ZA realizations. The solid lines show the results from single ZA realizations starting from the same density fields as the  $N$ -body simulations. The long dashed and short dashed curves are model fits for the ZA and dispersion model respectively. Only the first ten points have been used in constraining the ZA fits, and the first thirty for constraining the dispersion model. The corresponding best fit parameters and confidence intervals are shown Fig. 6.

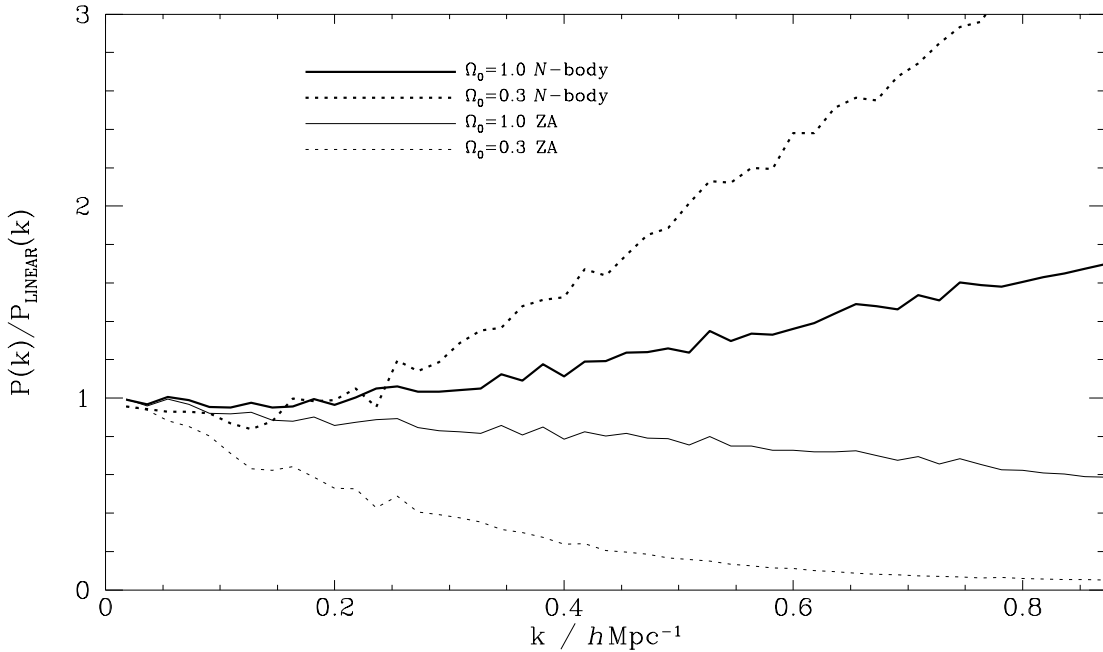


**Figure 4.** The ratio of estimates of the real-space evolved power spectra,  $P(k)$ , to the linear theory predictions,  $P_{\text{LINEAR}}(k)$ , for the  $N$ -body simulations and the corresponding ZA simulations. The models are the same  $\Omega_0 = 1$  and  $\Omega_0 = 0.3$  models studied in Fig. 3.



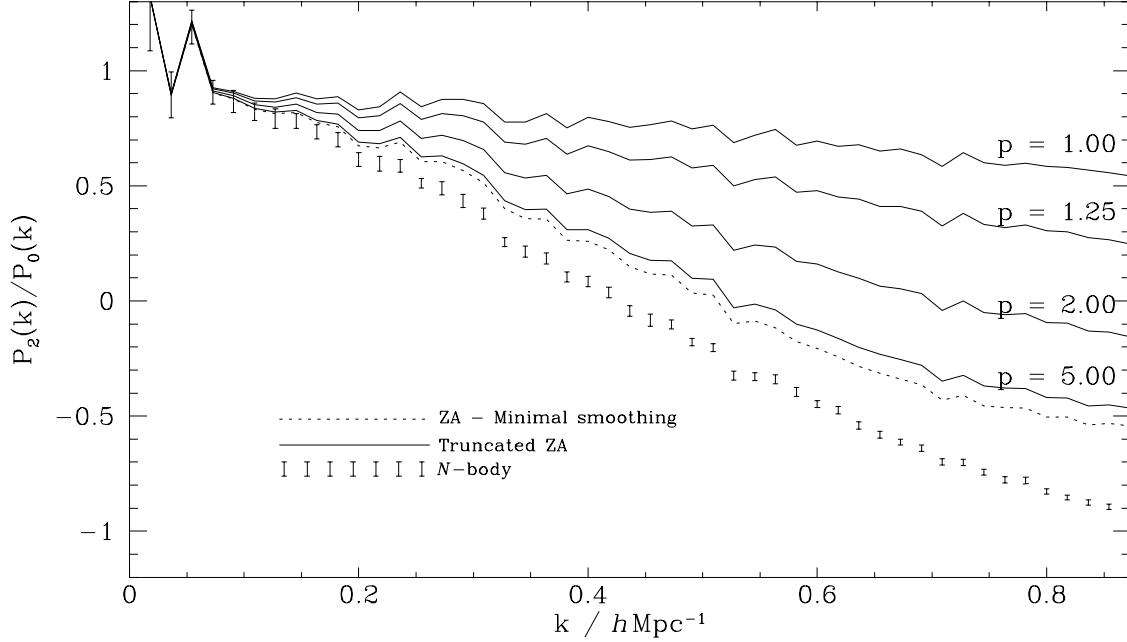


**Figure 5.** The dependence of the Zel'dovich approximation prediction for the ratio  $P_2(k)/P_0(k)$  on the extent to which the initial density field is smoothed before applying the ZA. The error bars show the  $N$ -body result for the  $\Omega_0 = 1.0$  model taken from Fig. 3. The dotted curve shows the ZA result for the minimal amount of smoothing, ie, truncation at the Nyquist frequency. The remaining curves show the effect of gradually increasing the smoothing using an additional Gaussian smoothing with  $k_s = pk_{nl}$  (see equation 4.9) and  $p = 5.0, 2.0, 1.25$  and  $1.0$ .

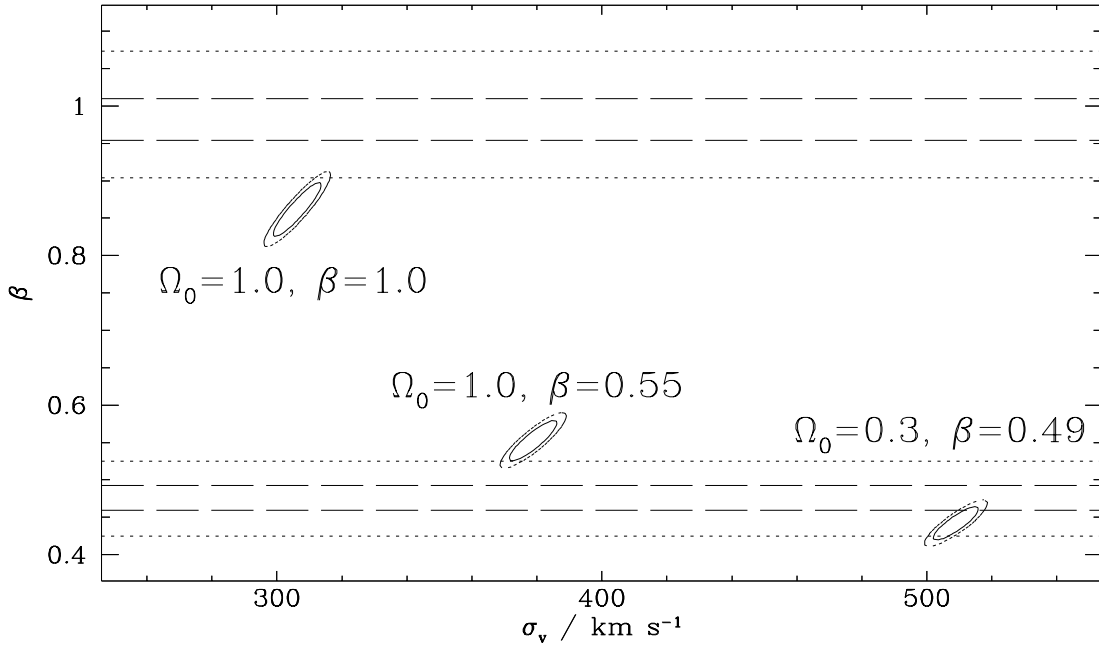


**Figure 6.** The 68% and 99.7% confidence intervals (1- & 3- $\sigma$ ) of the model parameters for the fits shown in Fig. 3 and Fig. 7. The ellipses are for the two-parameter dispersion model for the three different simulations, and the horizontal lines for single-parameter ZA model for the two unbiased models for which this provides a reasonably good fit. The best fit values of  $\beta$  and the  $\chi^2$  per degree of freedom for the best fit models are given in Table 1.

poor. Presumably the smoothing being applied is washing out the distortions we are trying to measure. However, we find that in real space a mild amount of smoothing can produce a power spectrum that is slightly closer to the  $N$ -body result, though this is a rather small effect.

The ZA and dispersion model fits are shown by the smooth long and short dashed curves in Fig. 3. The corresponding best fit model parameters and confidence intervals are shown in Fig. 6 and Table 1. Here the horizontal lines bracket the 68 per cent and 99.7 per cent ( $1$ - and  $3$ - $\sigma$ ) confidence intervals of  $\beta$  for the ZA fit. The ellipses show the corresponding confidence intervals for the two-parameter dispersion model. Both ZA fits give a best-fit  $\beta$  that is within  $1 - \sigma$  of the theoretical value, so there seems to be no appreciable systematic error in our estimate. However, this result is achieved by limiting the range of the fit to the first ten bins in  $k$ -space, ie.  $k < 0.182h \text{ Mpc}^{-1}$ , in both models. At smaller scales than this, particularly in the  $\Omega_0 = 1$  model, the fits can be seen to strongly overestimate the redshift-space distortion. Thus if a fit were made to data covering a wider range of scales,  $\beta$  would be severely underestimated. In contrast, the dispersion model fits remain in reasonable agreement with the data up to much larger  $k$ . We fit our data up to the thirtieth data bin, corresponding to a length scale of  $11.5h^{-1} \text{ Mpc}$ . For  $\Omega_0 = 0.3$ , the dispersion model analysis seems to be offset towards a low estimate of  $\beta$ , but this effect is fairly small given the size of the error contours. The fit itself is a very good over the whole range of  $k$  in question. However, for  $\Omega_0 = 1$ ,  $\beta$  is systematically underestimated by more than 10 per cent at a high level of significance. This offset can be understood by reference to the models shown in Fig. 2. In comparison to the ZA, which is an accurate fit at low- $k$ , the dispersion model curve changes slope too rapidly and is thus too shallow at low- $k$ . Thus, when data at low- $k$  are used to constrain the fit, the value of  $\beta$  is underestimated. We found this behaviour to be the same for a variant of the dispersion model in which the small scale random velocity is assumed to be Gaussian rather than exponentially distributed. This alternative Gaussian dispersion model produces a worse fit overall, and a more biased estimate of  $\beta$ . The same effect is also expected to introduce an offset in the  $\Omega_0 = 0.3$  simulation, but it is rather smaller for this case and so is not easily detected.

As shown in Table 1, we have calculated the 1-dimensional rms peculiar velocity of particles in each simulation,  $\sigma_v^{\text{SIM}}$ , in an attempt to look for a physical significance of the  $\sigma_v$  value found in the dispersion model fit. It is clear from these measurements that there is no simple relationship between the two quantities over the range covered by our simulations.

## 5.2 Biased Models

In Fig. 7 we show the model predictions for the quadrupole ratio,  $P_2(k)/P_0(k)$ , for a biased model with  $\Omega_0 = 1.0$ . The heavy curves show the results of selecting biased galaxy catalogues by the three methods described in Section 3.1. The differences between the models at large scales are purely statistical, since different galaxies have been selected in the different samples. At high  $k$  the two Lagrangian methods agree well, but the Eulerian one systematically shows less distortion. This is to be expected as this method populates evenly

$\Omega_0$	$\beta$	model	$\beta_{\text{fit}}$	$\chi^2/\nu$	$\sigma_v^{\text{FIT}}/\text{km s}^{-1}$	$\sigma_v^{\text{SIM}}/\text{km s}^{-1}$
1.0	1.00	ZA	0.98	2.28		
1.0	1.00	disp	0.87	2.03	306	381
0.3	0.49	ZA	0.48	0.86		
0.3	0.49	disp	0.44	0.99	509	442
1.0	0.55	disp	0.56	1.39	379	427

**Table 1.** Best fit  $\beta$  and goodness of fit ( $\chi^2$  per degree of freedom) indicator for our simulations under the Zel'dovich and dispersion models. For the dispersion model we also show the best fit values of  $\sigma_v$  and compare with the 1-dimensional velocity dispersion of the simulations,  $\sigma_v^{\text{SIM}}$ . Error contours for the fits are shown in Fig. 6.

all regions with density higher than the threshold, rather than giving extra weight to the areas with higher density (and thus velocity dispersion), as the other two models do.

The long dashed curve shows the prediction for the analytic ZA where, as suggested by FN96, the model adopted assumes that galaxies are unbiased,  $\sigma_8 = \sigma_8^{\text{gal}}$ , but with  $\Omega_0^{0.6} = 1/1.81$  to match the value of  $\beta = 1/b$ . This curve should be compared with the results from a biased catalogue constructed from a realization of the ZA which is shown by the thin solid curve. Clearly these two curves do not agree. Thus in the ZA, bias cannot be taken account of by merely modifying the value of  $f(\Omega_0)$  as suggested by FN96. This is perhaps to be expected as bias will not only boost the galaxy density fluctuations with respect to the underlying mass distribution, but will also preferentially place galaxies in dense structures where random velocities produced by virialized structures are largest. The small scale velocity field produced by shell crossing in the ZA is not a good model of the random velocities produced in non-linear regions. It is for this reason that the biased ZA realization is a poor fit to the  $N$ -body results. It diverges from the  $N$ -body result more rapidly than the corresponding model for the unbiased  $\Omega_0 = 1$  simulation.

The short dashed curve is a fit of the dispersion model to the  $N$ -body peaks biased galaxy catalogue. This model, with an exponential velocity distribution, determines  $\beta$  very accurately and is a good fit to the data over this range of scale. The fitted velocity dispersion is  $\sigma_v = 380 \text{ km s}^{-1}$ ,  $70 \text{ km s}^{-1}$  higher than the unbiased version of the same  $N$ -body simulation, which illustrates how bias preferentially places galaxies in environments with higher thermal velocities.

## 6 DISCUSSION

We have used a set of high resolution  $N$ -body simulations to investigate the accuracy of two models of the redshift-space distortion of galaxy clustering on scales of  $10$ – $200h^{-1} \text{ Mpc}$ . We conclude that neither the Zel'dovich Approximation (Fisher & Nusser 1996; Taylor & Hamilton 1996) nor the linear theory plus random velocity dispersion model (Peacock & Dodds 1994) provide an accurate description of redshift-space clustering. In general both models could lead to significant systematic errors in the estimation of  $\beta \equiv \Omega_0^{0.6}/b$  when applied to the high precision data that will be available from the large 2dF and SDSS galaxy redshift surveys.

The Zel'dovich Approximation provides a good fit in the

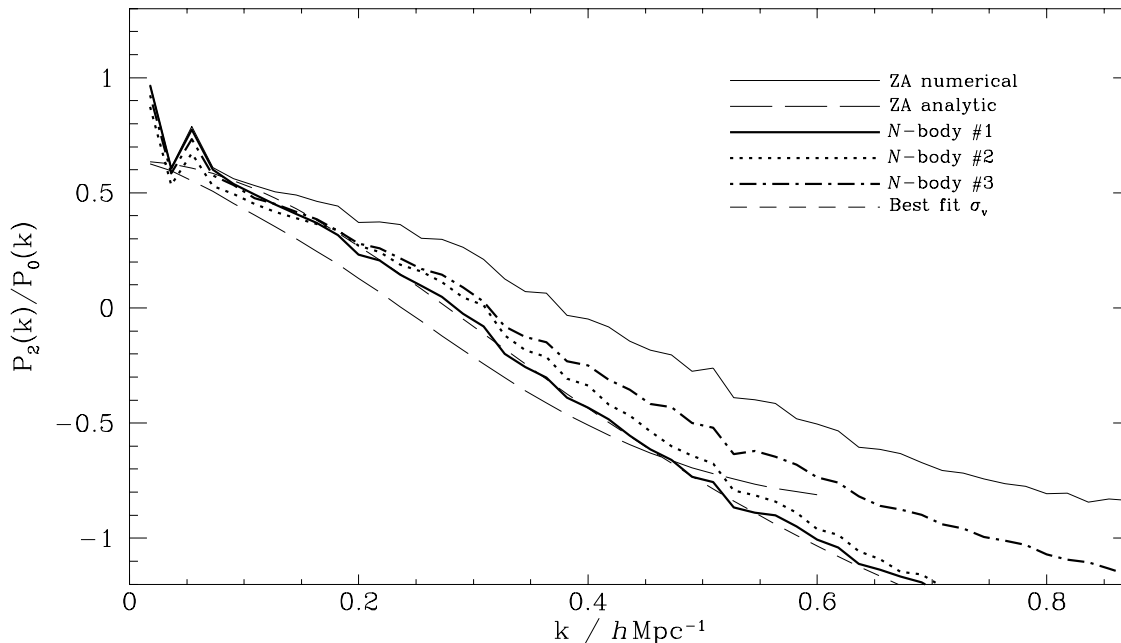


**Figure 7.** The quadrupole ratio,  $P_2(k)/P_0(k)$ , for biased  $\Omega_0 = 1$  galaxy catalogues with  $b = \sigma_8^{\text{gal}}/\sigma_8 = 1.81$ ,  $\beta = 0.55$ . The  $N$ -body lines show the results for our three different methods of constructing biased galaxy catalogues from the  $N$ -body simulation, as outlined in Section 3.1. The thin solid line shows the result of a ZA realization that has been biased in the same as one of the  $N$ -body catalogues. The long dashed curve shows the prediction of the ZA made by assuming  $\sigma_8 = \sigma_8^{\text{gal}}$  and  $\Omega_0^{0.6} = \beta$  as proposed by FN96. The short dashed line is a fit of the dispersion model to one of the  $N$ -body catalogues.

unbiased cases on the very largest scales that we have investigated. However, only for the low  $\Omega_0$  model that we examined does this model remain accurate over the full range of scales for which we measure a positive quadrupole distortion ( $P_2(k)/P_0(k) > 0$ ). In the case of biased galaxy catalogues the ZA is a very poor description of redshift clustering apart from on the very largest scales. Smoothing the initial density field prior to applying the ZA, as in the Truncated ZA (Melott, Pellman & Shandarin 1994), was found to further worsen the agreement with the  $N$ -body results of redshift-space distortions. In general, then, we would only advocate using the ZA for analysis of unbiased universes on scales down to  $\sim 40h^{-1}$  Mpc.

The two-parameter dispersion model was found to produce more acceptable fits to the  $N$ -body results. However, only in the cases in which the small scale velocity dispersion was large did these fits yield values of  $\beta$  that were not significantly biased with respect to the true values. This model also yields a value for the velocity dispersion parameter  $\sigma_v$ , but this depends on the degree and form of galaxy bias and so is difficult to directly relate to an interesting physical quantity. It should be noted that, although the dispersion model was unable to deal with the unbiased  $\Omega_0 = 1.0$  simulation, and in fact extracted a value of  $\beta$  offset from the true value by several-sigma, results from a variety of cosmological methods are making it seem increasingly unlikely that we live in such a universe – constraints from the observed  $\sigma_8$  and current  $\beta$  estimates require a low- $\Omega_0$  or biased cosmology. Thus the dispersion model may well prove to be a

useful tool for extracting information from redshift surveys on intermediate scales.

There appear to be two distinct ways to proceed to remedy or by-pass the above short-comings.

1) Improve the analytic models so as to produce accurate predictions over the full range of scales that will be probed by the redshift surveys.

A promising approach is an extension of the model discussed in Fisher (1995), where linear distortion effects on  $\xi(\sigma, \pi)$  are modelled as a convolution with a Gaussian velocity distribution with scale- and orientation-dependent velocity dispersion. Fisher suggests that this model may be adapted to deal with distortions in the highly non-linear regime by replacing the Gaussian with a generalized distribution function which is Gaussian on large scales but tends to an exponential with isotropic and constant velocity dispersion on small scales.

Hamilton et al. (1991) developed an accurate method of obtaining the non-linear correlation function in real space,  $\xi(r)$ , using a universal scaling relation. Mo, Jing, & Börner (1996) outline a technique by which the quantities which define the velocity field (ie. mean pairwise peculiar velocity,  $v_{12}(r)$ , pairwise peculiar velocity dispersion,  $\langle v_{12}^2(r) \rangle$ , and mean square peculiar velocity,  $\langle v_1^2 \rangle$ ), can be modelled for a given cosmology and initial power spectrum.

Given reliable models for these quantities, Fisher's treatment should provide a way of translating  $\xi(r)$  into the redshift space statistic  $\xi(\sigma, \pi)$ , and thus calculating precisely the anisotropy expected on any given scale. However, this method is still subject to problems – namely, finding out

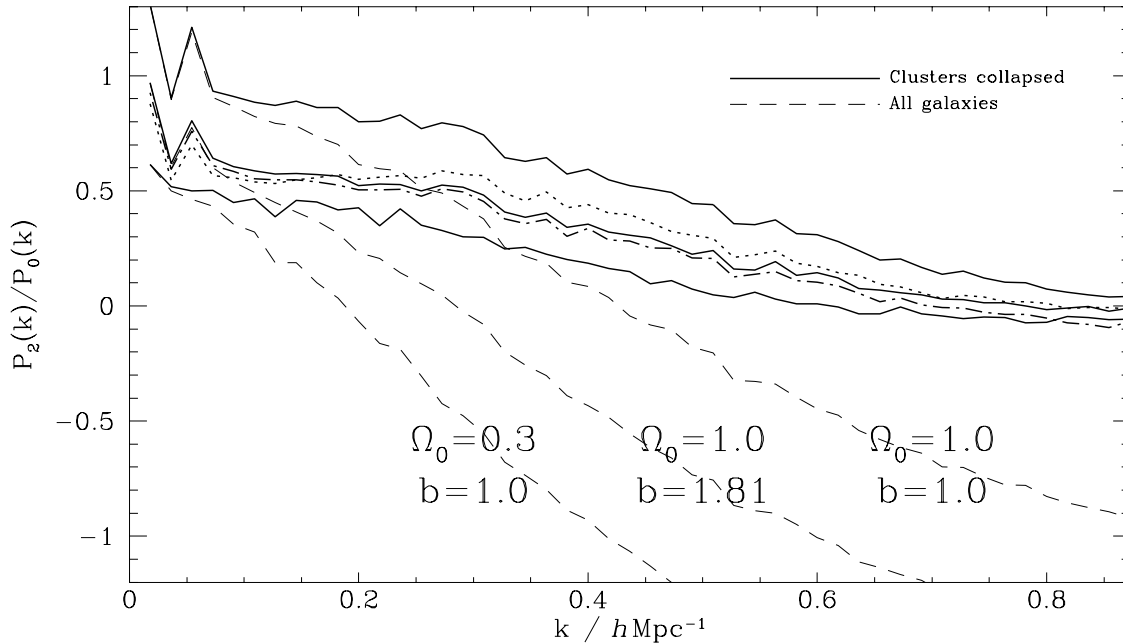


**Figure 8.** A comparison of the quadrupole ratio,  $P_2(k)/P_0(k)$  before and after identifying and collapsing the galaxy clusters. The dashed lines show the original shape for the three simulations, where we have used the peaks biasing method for the biased case. The solid lines the result after cluster collapse for the three models. We also plot the other two variants of the biasing model in the collapsed case, using a dotted line for method 2 and dot-dashed for method 3.

exactly how the velocity distribution function behaves on intermediate scales, and developing a way for modelling the effects of galaxy bias. We intend to investigate this in a future paper.

2) As our computers increase in memory and CPU power, the ‘brute force’ approach of simply running  $N$ -body simulations for the whole range of parameter space becomes increasingly plausible. Here the dispersion model may be very useful in fitting and suggesting the approximate value of  $\beta$ , and thus putting restrictions on the combinations of parameter values worth investigating.

If one is resorting to simulations then it may be possible to filter the data to remove some non-linearities before commencing the analysis of redshift-space distortions. An interesting procedure for doing this is to identify and collapse galaxy clusters. Since their high velocity dispersion is responsible for much of the suppression of  $P_2/P_0$ , their removal might lead to more robust estimates of  $\beta$ . Fig. 8 illustrates the effect of collapsing clusters in our simulations. As expected, the anisotropy is much closer to the linear theory prediction on large and intermediate scales. On small scales the quadrupole ratio converges on zero rather than becoming strongly negative. Cluster membership was established using a friends-of-friends algorithm, in which any pair of galaxies with separation less than 0.2 times the mean separation are classed as being in the same cluster. Each cluster member then has its velocity replaced with the mean velocity of the cluster itself, effectively eliminating the internal velocity dispersion of these virialized structures.

The identification of galaxy clusters will be much more complex when dealing with real galaxy redshift surveys.

Moore, Frenk & White (1993) describe a way of applying this technique to the CfA survey using a redshift- and orientation-dependent linking length to define groups. Whatever algorithm one adopts can always be tested by running it on mock galaxy catalogues made from the  $N$ -body simulations.

Despite the failings of existing models pointed out in this work, redshift-space distortion analysis remains very interesting and promises to be of great use in extracting information from the next generation of galaxy surveys.

## ACKNOWLEDGEMENTS

The authors wish to thank Carlos Frenk, David Weinberg and Scott Croom for some useful criticisms and Karl Fisher for advice on evaluating the Zel’dovich approximation integral. SC acknowledges the support of a PPARC Advanced Fellowship. SJH acknowledges the support of a PPARC Research Studentship.

## REFERENCES

- Bardeen J.M., Bond J.R., Kaiser N., Szalay A.S., 1986, *ApJ*, 304, 15
- Baugh C.M., Gaztañaga E., 1996, *MNRAS*, 280, L37
- Baugh C.M., Gaztañaga E., Efstathiou G., 1995, *MNRAS*, 274, 1049
- Bean A.J., Ellis R.S., Shanks T., Efstathiou G., Peterson B.A., 1983, *MNRAS*, 205, 605
- Bouchet F.R., Colombi S., Hivon E., Juszkiewicz R., 1995, *A&A*, 296, 575

- Bromley B.C., Warren M.S., Zurek W.H., 1997, ApJ, 475, 414  
 Cole S., Fisher K.B., Weinberg D.H., 1994, MNRAS, 267, 785  
 Cole S., Fisher K.B., Weinberg D.H., 1995, MNRAS, 275, 515  
 Cole S., Hatton S.J., Weinberg D.H., Frenk C.S., in preparation  
 Colless M., 1996, in proceedings of the Heron Island Conference,  
<http://msowwww.anu.edu.au/~heron/Colless/colless.html>  
 Couchman H.M.P., 1991, ApJ, 368, 23  
 da Costa L.N., Vogeley M.S., Geller M.J., Huchra J.P., Park C.,  
 1994, ApJ, 437, L1  
 Davis M., Peebles P.J.E., 1983, ApJ, 267, 465  
 Efstathiou G., Davis M., White S.D.M., Frenk C.S., 1985, ApJS,  
 57, 241  
 Eke V.R., Cole S., Frenk C.S., 1996, MNRAS, 282, 263  
 Feldman H.A., Kaiser N., Peacock J.A., 1994, ApJ, 426, 23  
 Fisher K.B., 1995, ApJ, 448, 494  
 Fisher K.B., Nusser A., 1996, MNRAS, 279, L1 **FN96**  
 Fisher K.B., Davis M., Strauss M.A., Yahil A., Huchra J.P., 1994,  
 MNRAS, 267, 927  
 Gorski K., 1988, ApJ, 332, L7  
 Gregory S.A., Thompson L.A., 1978, ApJ, 222, 784  
 Gunn J.E., Weinberg D.H., 1995, Wide-Field Spectroscopy and  
 the Distant Universe, proceedings of the 35th Herstmonceux  
 workshop, Cambridge University Press, Cambridge  
 Hamilton A.J.S., 1993, ApJ, 406, L47  
 Hamilton A.J.S., Kumar P., Lu E., Matthews A., 1991, ApJ, 374,  
 L1  
 Jackson J.C., 1972, MNRAS, 156, 1P  
 Kaiser N., 1987, MNRAS, 227, 1  
 Lin H., Kirshner R.P., Shectman S.A., Landy S.D., Oemler A.,  
 Tucker D.L., Schechter P.L., 1996, ApJ, 471, 617  
 Loveday J., Efstathiou G., Maddox S.J., Peterson B.A., 1996,  
 ApJ, 468, 1L  
 Maddox S.J., Efstathiou G., Sutherland W.J., 1996, MNRAS,  
 283, 1227  
 Melott A.L., Pellman T.E., Shandarin S.F., 1994, MNRAS, 269,  
 626  
 Mo H.J., Jing Y.P., Börner G., 1996, Preprint MPA 992, Max-  
 Planck-Institut Für Astrophysik  
 Moore, B., Frenk C.S., White S.D.M., 1993, MNRAS, 261, 827  
 Park C., Vogeley M.S., Geller M.J., Huchra J.P., 1994, ApJ, 431,  
 569  
 Peacock J.A., Dodds S.J., 1994, MNRAS, 267, 1020  
 Peebles P.J.E., 1993, Principles of Physical Cosmology. Princeton  
 University Press, Princeton  
 Press W.H., Teukolsky S.A., Vetterling W.T., Flannery B.P., Nu-  
 merical Recipes in FORTRAN, 2nd edition. Cambridge Uni-  
 versity Press, Cambridge  
 Ratcliffe A., Shanks T., Fong R., Parker Q.A., 1997a, MNRAS  
 submitted  
 Ratcliffe A., Shanks T., Fong R., Parker Q.A., 1997b, MNRAS  
 submitted  
 Sargent W.W., Turner E.L., 1977, ApJ, 212, L3  
 Smoot G., et al., 1992, ApJ, 396, L1  
 Strauss M.A., Willick J.A., 1995, Physics Reports, 261, 271  
 Tadros H., Efstathiou G., 1995, MNRAS, 276, 45  
 Taylor A.N., Hamilton A.J.S., 1996, MNRAS, 282, 767  
 Weinberg D.H., Cole S., 1992, MNRAS, 259, 652  
 White S.D.M., 1994, Les Houches Lectures (astro-ph/9410043)  
 White S.D.M., Efstathiou G., Frenk C.S., 1993, MNRAS, 262,  
 1023  
 White S.D.M., Frenk C.S., Davis M., Efstathiou G., 1987, ApJ,  
 313, 505  
 Zel'dovich Ya.B., 1970, A&A, 5, 84